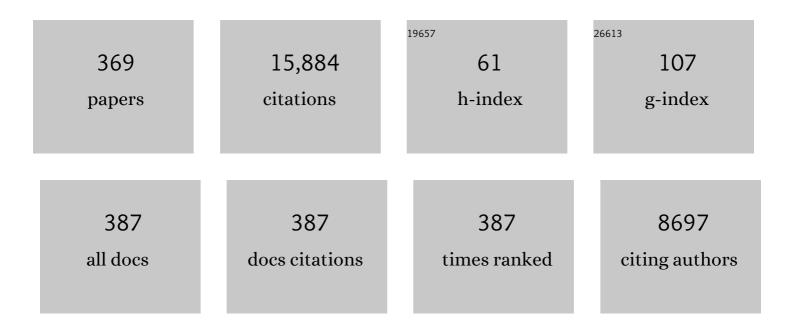
Baptiste Gault

List of Publications by Year in descending order

Source: https://exaly.com/author-pdf/4757664/publications.pdf Version: 2024-02-01



RADTISTE CALLET

#	Article	IF	CITATIONS
1	Multidimensional thermally-induced transformation of nest-structured complex Au-Fe nanoalloys towards equilibrium. Nano Research, 2022, 15, 581-592.	10.4	16
2	Three-Dimensional Atomically Resolved Analytical Imaging with a Field Ion Microscope. Microscopy and Microanalysis, 2022, 28, 1264-1279.	0.4	5
3	Mechanisms of austenite growth during intercritical annealing in medium manganese steels. Scripta Materialia, 2022, 206, 114228.	5.2	27
4	A Liquid Metal Encapsulation for Analyzing Porous Nanomaterials by Atom Probe Tomography. Microscopy and Microanalysis, 2022, 28, 1198-1206.	0.4	5
5	Dynamic strain aging in the intermediate temperature regime of near- <mml:math xmlns:mml="http://www.w3.org/1998/Math/MathML" altimg="si14.svg"><mml:mi>α</mml:mi> titanium alloy, IMI 834: Experimental and modeling. Acta Materialia, 2022, 222, 117436.</mml:math 	7.9	18
6	Reflections on the Spatial Performance of Atom Probe Tomography in the Analysis of Atomic Neighborhoods. Microscopy and Microanalysis, 2022, 28, 1116-1126.	0.4	16
7	Grain boundary segregation and its implications regarding the formation of the grain boundary α phase in the metastable l²-Titanium Ti–5Al–5Mo–5V–3Cr alloy. Scripta Materialia, 2022, 207, 114320.	5.2	28
8	Microstructure manipulation by laser-surface remelting of a full-Heusler compound to enhance thermoelectric properties. Acta Materialia, 2022, 223, 117501.	7.9	7
9	Quantitative analysis of grain boundary diffusion, segregation and precipitation at a sub-nanometer scale. Acta Materialia, 2022, 225, 117522.	7.9	18
10	Measuring oxygen solubility in Ni grains and boundaries after oxidation using atom probe tomography. Scripta Materialia, 2022, 210, 114411.	5.2	6
11	Grain boundary in NbCo(Pt)Sn half-Heusler compounds: Segregation and solute drag on grain boundary migration. Acta Materialia, 2022, 226, 117604.	7.9	5
12	Revealing in-plane grain boundary composition features through machine learning from atom probe tomography data. Acta Materialia, 2022, 226, 117633.	7.9	9
13	Status and Direction of Atom Probe Analysis of Frozen Liquids. Microscopy and Microanalysis, 2022, 28, 1150-1167.	0.4	8
14	Atom probe analysis of electrode materials for Li-ion batteries: challenges and ways forward. Journal of Materials Chemistry A, 2022, 10, 4926-4935.	10.3	20
15	Origins of the hydrogen signal in atom probe tomography: case studies of alkali and noble metals. New Journal of Physics, 2022, 24, 013008.	2.9	10
16	Understanding Alkali Contamination in Colloidal Nanomaterials to Unlock Grain Boundary Impurity Engineering. Journal of the American Chemical Society, 2022, 144, 987-994.	13.7	12
17	Hierarchical nature of hydrogen-based direct reduction of iron oxides. Scripta Materialia, 2022, 213, 114571.	5.2	43
18	A cracking oxygen story: A new view of stress corrosion cracking in titanium alloys. Acta Materialia, 2022, 227, 117687.	7.9	17

#	Article	IF	CITATIONS
19	Laser-equipped gas reaction chamber for probing environmentally sensitive materials at near atomic scale. PLoS ONE, 2022, 17, e0262543.	2.5	7
20	Hydrogen trapping and embrittlement in high-strength Al alloys. Nature, 2022, 602, 437-441.	27.8	109
21	Massive interstitial solid solution alloys achieve near-theoretical strength. Nature Communications, 2022, 13, 1102.	12.8	29
22	Effect of Nb micro-alloying on austenite nucleation and growth in a medium manganese steel during intercritical annealing. Acta Materialia, 2022, 229, 117786.	7.9	24
23	In-situ synchrotron-based high energy X-ray diffraction study of the deformation mechanism of Î'-hydrides in a commercially pure titanium. Scripta Materialia, 2022, 213, 114608.	5.2	5
24	The role of β pockets resulting from Fe impurities in hydride formation in titanium. Scripta Materialia, 2022, 213, 114640.	5.2	1
25	The effect of hydrogen on the multiscale mechanical behaviour of a La(Fe,Mn,Si)13-based magnetocaloric material. Journal of Alloys and Compounds, 2022, 906, 164274.	5.5	10
26	A sustainable ultra-high strength Fe18Mn3Ti maraging steel through controlled solute segregation and α-Mn nanoprecipitation. Nature Communications, 2022, 13, 2330.	12.8	22
27	Bubbles and atom clusters in rock melts: A chicken and egg problem. Journal of Volcanology and Geothermal Research, 2022, 428, 107574.	2.1	6
28	Controlled Doping of Electrocatalysts through Engineering Impurities. Advanced Materials, 2022, 34, e2203030.	21.0	12
29	Suppressed hydrogen embrittlement of high-strength Al alloys by Mn-rich intermetallic compound particles. Acta Materialia, 2022, 236, 118110.	7.9	22
30	The effect of Î ³ matrix channel width on the compositional evolution in a multi-component nickel-based superalloy. Scripta Materialia, 2022, 219, 114853.	5.2	2
31	Hydriding of titanium: Recent trends and perspectives in advanced characterization and multiscale modeling. Current Opinion in Solid State and Materials Science, 2022, 26, 101020.	11.5	15
32	A model to predict image formation in the three-dimensional field ion microscope. Computer Physics Communications, 2021, 260, 107317.	7.5	9
33	Beyond Solid Solution Highâ€Entropy Alloys: Tailoring Magnetic Properties via Spinodal Decomposition. Advanced Functional Materials, 2021, 31, 2007668.	14.9	51
34	Carbon redistribution in quenched and tempered lath martensite. Acta Materialia, 2021, 205, 116521.	7.9	60
35	Properties and influence of microstructure and crystal defects in Fe2VAl modified by laser surface remelting. Scripta Materialia, 2021, 193, 153-157.	5.2	16
36	Nucleation mechanism of hetero-epitaxial recrystallization in wrought nickel-based superalloys. Scripta Materialia, 2021, 191, 7-11.	5.2	23

#	Article	IF	CITATIONS
37	Enhanced creep performance in a polycrystalline superalloy driven by atomic-scale phase transformation along planar faults. Acta Materialia, 2021, 202, 232-242.	7.9	29
38	Multiscale analysis of grain boundary microstructure in high strength 7xxx Al alloys. Acta Materialia, 2021, 202, 190-210.	7.9	47
39	Effect of interface dislocations on mass flow during high temperature and low stress creep of single crystal Ni-base superalloys. Scripta Materialia, 2021, 191, 23-28.	5.2	28
40	Machine-learning-enhanced time-of-flight mass spectrometry analysis. Patterns, 2021, 2, 100192.	5.9	14
41	Fluid inclusion induced hardening: nanoscale evidence from naturally deformed pyrite. Contributions To Mineralogy and Petrology, 2021, 176, 1.	3.1	10
42	Hydride growth mechanism in zircaloy-4: Investigation of the partitioning of alloying elements. Materialia, 2021, 15, 101006.	2.7	14
43	Microstructure formation and mechanical properties of ODS steels built by laser additive manufacturing of nanoparticle coated iron-chromium powders. Acta Materialia, 2021, 206, 116566.	7.9	67
44	Elemental Sub-Lattice Occupation and Microstructural Evolution in γ/γ′ Co–12Ti–4Mo–Cr Alloys. Microscopy and Microanalysis, 2021, , 1-5.	0.4	0
45	The hidden structure dependence of the chemical life of dislocations. Science Advances, 2021, 7, .	10.3	24
46	A model to unravel the beneficial contributions of trace Cu in wrought Al–Mg alloys. Acta Materialia, 2021, 208, 116734.	7.9	9
47	Eutectoid growth of nanoscale amorphous Fe-Si nitride upon nitriding. Acta Materialia, 2021, 209, 116774.	7.9	6
48	Precipitation formation on â~5 and â~7 grain boundaries in 316L stainless steel and their roles on intergranular corrosion. Acta Materialia, 2021, 210, 116822.	7.9	30
49	Nbâ€Mediated Grain Growth and Grainâ€Boundary Engineering in Mg ₃ Sb ₂ â€Based Thermoelectric Materials. Advanced Functional Materials, 2021, 31, 2100258.	14.9	53
50	Influence of crystalline defects on magnetic nanodomains in a rare-earth-free magnetocrystalline anisotropic alloy. Physical Review Materials, 2021, 5, .	2.4	4
51	3D sub-nanometer analysis of glucose in an aqueous solution by cryo-atom probe tomography. Scientific Reports, 2021, 11, 11607.	3.3	10
52	Mechanisms of Ti <mml:math <br="" xmlns:mml="http://www.w3.org/1998/Math/MathML">altimg="si9.svg"><mml:msub><mml:mrow></mml:mrow><mml:mn>3</mml:mn></mml:msub></mml:math> Al precipitation in hcp <mml:math <br="" xmlns:mml="http://www.w3.org/1998/Math/MathML">altimg="si1.svg"><mml:mi>α</mml:mi></mml:math> -Ti. Acta Materialia, 2021, 212, 116811.	7.9	19
53	Correlating advanced microscopies reveals atomic-scale mechanisms limiting lithium-ion battery lifetime. Nature Communications, 2021, 12, 3740.	12.8	6
54	Influence of microstructure and atomic-scale chemistry on the direct reduction of iron ore with hydrogen at 700°C. Acta Materialia, 2021, 212, 116933.	7.9	61

#	Article	IF	CITATIONS
55	Partitioning of Solutes at Crystal Defects in Borides After Creep and Annealing in a Polycrystalline Superalloy. Jom, 2021, 73, 2293-2302.	1.9	3
56	Effect of Cd diffusion on the electrical properties of the Cu(In,Ga)Se2 thin-film solar cell. Solar Energy Materials and Solar Cells, 2021, 224, 110989.	6.2	12
57	Sustainable steel through hydrogen plasma reduction of iron ore: Process, kinetics, microstructure, chemistry. Acta Materialia, 2021, 213, 116971.	7.9	46
58	Atom probe tomography. Nature Reviews Methods Primers, 2021, 1, .	21.2	131
59	Chemical heterogeneity enhances hydrogen resistance in high-strength steels. Nature Materials, 2021, 20, 1629-1634.	27.5	83
60	Twins – A weak link in the magnetic hardening of ThMn12-type permanent magnets. Acta Materialia, 2021, 214, 116968.	7.9	31
61	CALPHAD-informed phase-field modeling of grain boundary microchemistry and precipitation in Al-Zn-Mg-Cu alloys. Acta Materialia, 2021, 214, 116966.	7.9	30
62	Understanding creep of a single-crystalline Co-Al-W-Ta superalloy by studying the deformation mechanism, segregation tendency and stacking fault energy. Acta Materialia, 2021, 214, 117019.	7.9	23
63	Analytical Three-Dimensional Field Ion Microscopy of an Amorphous Glass FeBSi. Microscopy and Microanalysis, 2021, , 1-9.	0.4	2
64	Dopant-segregation to grain boundaries controls electrical conductivity of n-type NbCo(Pt)Sn half-Heusler alloy mediating thermoelectric performance. Acta Materialia, 2021, 217, 117147.	7.9	24
65	High diffusivity pathways govern massively enhanced oxidation during tribological sliding. Acta Materialia, 2021, 221, 117353.	7.9	11
66	Reactive wear protection through strong and deformable oxide nanocomposite surfaces. Nature Communications, 2021, 12, 5518.	12.8	70
67	Discovery and Implications of Hidden Atomic-Scale Structure in a Metallic Meteorite. Nano Letters, 2021, 21, 8135-8142.	9.1	4
68	Open and strong-scaling tools for atom-probe crystallography: high-throughput methods for indexing crystal structure and orientation. Journal of Applied Crystallography, 2021, 54, 1490-1508.	4.5	0
69	Revealing atomic-scale vacancy-solute interaction in nickel. Scripta Materialia, 2021, 203, 114036.	5.2	7
70	On strong-scaling and open-source tools for analyzing atom probe tomography data. Npj Computational Materials, 2021, 7, .	8.7	14
71	Magnetoelectric Tuning of Pinningâ€Type Permanent Magnets through Atomicâ€Scale Engineering of Grain Boundaries. Advanced Materials, 2021, 33, 2006853.	21.0	13
72	Aluminum depletion induced by co-segregation of carbon and boron in a bcc-iron grain boundary. Nature Communications, 2021, 12, 6008.	12.8	24

#	Article	IF	CITATIONS
73	Substantially enhanced plasticity of bulk metallic glasses by densifying local atomic packing. Nature Communications, 2021, 12, 6582.	12.8	51
74	On the formation of hierarchical microstructure in a Mo-doped NiCoCr medium-entropy alloy with enhanced strength-ductility synergy. Scripta Materialia, 2020, 175, 1-6.	5.2	75
75	Electronic structure based design of thin film metallic glasses with superior fracture toughness. Materials and Design, 2020, 186, 108327.	7.0	13
76	Control of thermally stable core-shell nano-precipitates in additively manufactured Al-Sc-Zr alloys. Additive Manufacturing, 2020, 32, 100910.	3.0	27
77	Direct Imaging of Dopant and Impurity Distributions in 2D MoS ₂ . Advanced Materials, 2020, 32, e1907235.	21.0	26
78	Atomic‣cale Mapping of Impurities in Partially Reduced Hollow TiO ₂ Nanowires. Angewandte Chemie - International Edition, 2020, 59, 5651-5655.	13.8	42
79	Probing catalytic surfaces by correlative scanning photoemission electron microscopy and atom probe tomography. Journal of Materials Chemistry A, 2020, 8, 388-400.	10.3	19
80	Revealing nano-chemistry at lattice defects in thermoelectric materials using atom probe tomography. Materials Today, 2020, 32, 260-274.	14.2	73
81	On the atomic solute diffusional mechanisms during compressive creep deformation of a Co-Al-W-Ta single crystal superalloy. Acta Materialia, 2020, 184, 86-99.	7.9	45
82	Could face-centered cubic titanium in cold-rolled commercially-pure titanium only be a Ti-hydride?. Scripta Materialia, 2020, 178, 39-43.	5.2	36
83	Effect of nanoparticle additivation on the microstructure and microhardness of oxide dispersion strengthened steels produced by laser powder bed fusion and directed energy deposition. Procedia CIRP, 2020, 94, 41-45.	1.9	16
84	Nanocrystalline Sm-based 1:12 magnets. Acta Materialia, 2020, 200, 652-658.	7.9	26
85	Extensive nanoprecipitate morphology transformation in a nanostructured ferritic alloy due to extreme thermomechanical processing. Acta Materialia, 2020, 200, 922-931.	7.9	11
86	Different Photostability of BiVO ₄ in Near-pH-Neutral Electrolytes. ACS Applied Energy Materials, 2020, 3, 9523-9527.	5.1	41
87	In-situ synthesis via laser metal deposition of a lean Cu–3.4Cr–0.6Nb (at%) conductive alloy hardened by Cr nano-scale precipitates and by Laves phase micro-particles. Acta Materialia, 2020, 197, 330-340.	7.9	30
88	Thermoelectric properties of n-type half-Heusler NbCoSn with heavy-element Pt substitution. Journal of Materials Chemistry A, 2020, 8, 14822-14828.	10.3	44
89	Microstructural Evolution in an Fe-10Ni-0.1C Steel During Heat Treatment and High Strain-Rate Deformation. Metallurgical and Materials Transactions A: Physical Metallurgy and Materials Science, 2020, 51, 5056-5076.	2.2	4
90	Crystal–Glass Highâ€Entropy Nanocomposites with Near Theoretical Compressive Strength and Large Deformability. Advanced Materials, 2020, 32, e2002619.	21.0	66

#	Article	IF	CITATIONS
91	Intermixing of Fe and Cu on the atomic scale by high-pressure torsion as revealed by DC- and AC-SQUID susceptometry and atom probe tomography. Acta Materialia, 2020, 196, 210-219.	7.9	11
92	Dynamic Effects in Voltage Pulsed Atom Probe. Microscopy and Microanalysis, 2020, 26, 1133-1146.	0.4	6
93	Analysis of nanoscale fluid inclusions in geomaterials by atom probe tomography: Experiments and numerical simulations. Ultramicroscopy, 2020, 218, 113092.	1.9	8
94	Reversion and re-aging of a peak aged Al-Zn-Mg-Cu alloy. Scripta Materialia, 2020, 188, 269-273.	5.2	37
95	Nanoglass–Nanocrystal Composite—a Novel Material Class for Enhanced Strength–Plasticity Synergy. Small, 2020, 16, e2004400.	10.0	12
96	Current Challenges and Opportunities in Microstructure-Related Properties of Advanced High-Strength Steels. Metallurgical and Materials Transactions A: Physical Metallurgy and Materials Science, 2020, 51, 5517-5586.	2.2	115
97	Segregation-assisted spinodal and transient spinodal phase separation at grain boundaries. Npj Computational Materials, 2020, 6, .	8.7	29
98	Enabling near-atomic–scale analysis of frozen water. Science Advances, 2020, 6, .	10.3	41
99	Controlling the Oxidation of Magnetic and Electrically Conductive Solid-Solution Iron-Rhodium Nanoparticles Synthesized by Laser Ablation in Liquids. Nanomaterials, 2020, 10, 2362.	4.1	18
100	Application of SIMS and APT to Understand Scale Dependent U-Pb Isotope Behavior in Zircon. Microscopy and Microanalysis, 2020, 26, 2994-2995.	0.4	0
101	On the rhenium segregation at the low angle grain boundary in a single crystal Ni-base superalloy. Scripta Materialia, 2020, 185, 88-93.	5.2	29
102	High-rate superplasticity in an equiatomic medium-entropy VCoNi alloy enabled through dynamic recrystallization of a duplex microstructure of ordered phases. Acta Materialia, 2020, 194, 106-117.	7.9	57
103	High-strength Damascus steel by additive manufacturing. Nature, 2020, 582, 515-519.	27.8	260
104	Lattice Oxygen Exchange in Rutile IrO ₂ during the Oxygen Evolution Reaction. Journal of Physical Chemistry Letters, 2020, 11, 5008-5014.	4.6	81
105	The effect of solute segregation to deformation twin boundaries on the electrical resistivity of a single-phase superalloy. Scripta Materialia, 2020, 186, 208-212.	5.2	12
106	Plasticity assisted redistribution of solutes leading to topological inversion during creep of superalloys. Scripta Materialia, 2020, 186, 287-292.	5.2	26
107	Snoek-type damping performance in strong and ductile high-entropy alloys. Science Advances, 2020, 6, eaba7802.	10.3	56
108	Chemical segregation and precipitation at anti-phase boundaries in thermoelectric Heusler-Fe2VAl. Scripta Materialia, 2020, 186, 370-374.	5.2	9

#	Article	IF	CITATIONS
109	Reflections on the Analysis of Interfaces and Grain Boundaries by Atom Probe Tomography. Microscopy and Microanalysis, 2020, 26, 247-257.	0.4	30
110	Interplay of Chemistry and Faceting at Grain Boundaries in a Model Al Alloy. Physical Review Letters, 2020, 124, 106102.	7.8	25
111	The effect of Zr on precipitation in oxide dispersion strengthened FeCrAl alloys. Journal of Nuclear Materials, 2020, 533, 152105.	2.7	21
112	Spinodal decomposition in alkali feldspar studied by atom probe tomography. Physics and Chemistry of Minerals, 2020, 47, 30.	0.8	6
113	On the chemistry of grain boundaries in CuInS2 films. Nano Energy, 2020, 76, 105081.	16.0	11
114	Solute hydrogen and deuterium observed at the near atomic scale in high-strength steel. Acta Materialia, 2020, 188, 108-120.	7.9	64
115	Crack initiation mechanisms during very high cycle fatigue of Ni-based single crystal superalloys at high temperature. Acta Materialia, 2020, 188, 131-144.	7.9	112
116	Nanoscale compositional fluctuations enabled by dynamic strain-induced austenite reversion in a Mn-rich duplex steel. Scripta Materialia, 2020, 181, 101-107.	5.2	7
117	(Al, Zn)3Zr dispersoids assisted η′ precipitation in anAl-Zn-Mg-Cu-Zr alloy. Materialia, 2020, 10, 100641.	2.7	28
118	Interpreting nanovoids in atom probe tomography data for accurate local compositional measurements. Nature Communications, 2020, 11, 1022.	12.8	23
119	Metrology of small particles and solute clusters by atom probe tomography. Acta Materialia, 2020, 188, 406-415.	7.9	83
120	Cryo-focused ion beam preparation of perovskite based solar cells for atom probe tomography. PLoS ONE, 2020, 15, e0227920.	2.5	26
121	Ptlr protective coating system for precision glass molding tools: Design, evaluation and mechanism of degradation. Surface and Coatings Technology, 2020, 385, 125378.	4.8	19
122	Unveiling the Re effect in Ni-based single crystal superalloys. Nature Communications, 2020, 11, 389.	12.8	101
123	New approach for FIB-preparation of atom probe specimens for aluminum alloys. PLoS ONE, 2020, 15, e0231179.	2.5	26
124	Formation of a 2D Meta-stable Oxide by Differential Oxidation of AgCu Alloys. ACS Applied Materials & Interfaces, 2020, 12, 23595-23605.	8.0	9
125	An atom probe tomography and inventory calculation examination of second phase precipitates in neutron irradiated single crystal tungsten. Nuclear Fusion, 2020, 60, 126013.	3.5	20
126	Grain boundary segregation, phase formation, and their influence on the coercivity of rapidly solidified SmFe11Ti hard magnetic alloys. Physical Review Materials, 2020, 4, .	2.4	6

#	Article	IF	CITATIONS
127	Atomic Structure and Chemical Composition of Planar Fault Structures in Co-Base Superalloys. Minerals, Metals and Materials Series, 2020, , 920-928.	0.4	2
128	Grain boundary segregation and precipitation in an Al-Zn-Mg-Cu alloy. MATEC Web of Conferences, 2020, 326, 01004.	0.2	0
129	Atomic‣cale Mapping of Impurities in Partially Reduced Hollow TiO 2 Nanowires. Angewandte Chemie, 2020, 132, 5700-5704.	2.0	3
130	Tuning Fundamental Properties of Ir-Based Materials to Enhance Their Electrocatalytic Performance in the Oxygen Evolution Reaction. ECS Meeting Abstracts, 2020, MA2020-01, 1557-1557.	0.0	0
131	Atomic-Scale View into the Degradation of Ir-Ru Alloys during Anodic Oxygen Evolution. ECS Meeting Abstracts, 2020, MA2020-01, 1520-1520.	0.0	Ο
132	Prospects of Making Nanoporous Ruthenium from Transition Metal-Ru Alloys. ECS Meeting Abstracts, 2020, MA2020-01, 2713-2713.	0.0	0
133	New Frontiers in Electrocatalyst Characterization – Three Dimensional Atomic-Scale Insights By Atom Probe Tomography. ECS Meeting Abstracts, 2020, MA2020-01, 2561-2561.	0.0	Ο
134	Interface characteristics in an <mml:math xmlns:mml="http://www.w3.org/1998/Math/MathML"><mml:mrow><mml:mi>α</mml:mi><mml:mo>+titanium alloy. Physical Review Materials, 2020, 4, .</mml:mo></mml:mrow></mml:math 	no> 2.4 1ml:ı	mi>Ĵi²
135	(Invited) From Atomic-Scale Understanding to Design of Advanced Electrocatalyst Materials. ECS Meeting Abstracts, 2020, MA2020-02, 3154-3154.	0.0	Ο
136	Cryo-focused ion beam preparation of perovskite based solar cells for atom probe tomography. , 2020, 15, e0227920.		0
137	Cryo-focused ion beam preparation of perovskite based solar cells for atom probe tomography. , 2020, 15, e0227920.		Ο
138	Cryo-focused ion beam preparation of perovskite based solar cells for atom probe tomography. , 2020, 15, e0227920.		0
139	Cryo-focused ion beam preparation of perovskite based solar cells for atom probe tomography. , 2020, 15, e0227920.		Ο
140	New approach for FIB-preparation of atom probe specimens for aluminum alloys. , 2020, 15, e0231179.		0
141	New approach for FIB-preparation of atom probe specimens for aluminum alloys. , 2020, 15, e0231179.		Ο
142	New approach for FIB-preparation of atom probe specimens for aluminum alloys. , 2020, 15, e0231179.		0
143	New approach for FIB-preparation of atom probe specimens for aluminum alloys. , 2020, 15, e0231179.		0
144	New approach for FIB-preparation of atom probe specimens for aluminum alloys. , 2020, 15, e0231179.		0

#	Article	IF	CITATIONS
145	New approach for FIB-preparation of atom probe specimens for aluminum alloys. , 2020, 15, e0231179.		Ο
146	Correlative Microscopy Observation (3D EBSD + APT + TEM) on Intergranular Corrosion Behaviors in 316L Stainless Steel. Microscopy and Microanalysis, 2019, 25, 748-749.	0.4	2
147	Combined APT, TEM and SAXS Characterisation of Nanometre-Scale Precipitates in Titanium Alloys. Microscopy and Microanalysis, 2019, 25, 2516-2517.	0.4	1
148	Direct atomic insight into the role of dopants in phase-change materials. Nature Communications, 2019, 10, 3525.	12.8	56
149	Quantification of Solute Deuterium in Titanium Deuteride by Atom Probe Tomography with Both Laser Pulsing and High-Voltage Pulsing: Influence of the Global and Local Surface Electric Field. Microscopy and Microanalysis, 2019, 25, 2512-2513.	0.4	Ο
150	New Applications to Atom Probe Tomography: Insights on Trace Element Diffusion in Naturally Deformed Minerals. Microscopy and Microanalysis, 2019, 25, 2498-2499.	0.4	0
151	Segregation-driven grain boundary spinodal decomposition as a pathway for phase nucleation in a high-entropy alloy. Acta Materialia, 2019, 178, 1-9.	7.9	102
152	Deformation of Borides in Nickel-based Superalloys: a Study of Segregation at Dislocations. Microscopy and Microanalysis, 2019, 25, 2538-2539.	0.4	4
153	Carbon partitioning and microstructure evolution during tempering of an Fe-Ni-C steel. Scripta Materialia, 2019, 172, 38-42.	5.2	12
154	Atomic-scale grain boundary engineering to overcome hot-cracking in additively-manufactured superalloys. Acta Materialia, 2019, 177, 209-221.	7.9	165
155	Light, strong and cost effective: Martensitic steels based on the Fe – Al – C system. Materials Science & Engineering A: Structural Materials: Properties, Microstructure and Processing, 2019, 762, 138088.	5.6	7
156	Atomistic phase field chemomechanical modeling of dislocation-solute-precipitate interaction in Ni–Al–Co. Acta Materialia, 2019, 175, 250-261.	7.9	51
157	On Strong Scaling Open Source Tools for Mining Atom Probe Tomography Data. Microscopy and Microanalysis, 2019, 25, 298-299.	0.4	2
158	Application of Atom Probe Tomography to Complex Microstructures of Laser Additively Manufactured Samples. Microscopy and Microanalysis, 2019, 25, 2514-2515.	0.4	0
159	An Integrated Workflow To Investigate Electrocatalytic Surfaces By Correlative X-ray Photoemission Spectroscopy, Scanning Photoemission Electron Microscopy and Atom Probe Tomography. Microscopy and Microanalysis, 2019, 25, 306-307.	0.4	1
160	Hydride Growth Mechanism in Zircaloy-4: Investigation of the Partitioning of Alloying Elements. Microscopy and Microanalysis, 2019, 25, 2506-2507.	0.4	0
161	Hough Transform Based Accurate Composition Extractions From Correlation Histograms in Atom Probe Tomography. Microscopy and Microanalysis, 2019, 25, 324-325.	0.4	1
162	A 2D and 3D nanostructural study of naturally deformed pyrite: assessing the links between trace element mobility and defect structures. Contributions To Mineralogy and Petrology, 2019, 174, 1.	3.1	24

#	Article	IF	CITATIONS
163	An Atomic Renaissance For Pulsed Field Ion Microscopy. Microscopy and Microanalysis, 2019, 25, 304-305.	0.4	0
164	Direct Observation of Hydrogen in Cold-Drawn Pearlitic Steel Wires Using Cryogenic Atom Probe Tomography. Microscopy and Microanalysis, 2019, 25, 2522-2523.	0.4	1
165	Additive manufacturing of CMSX-4 Ni-base superalloy by selective laser melting: Influence of processing parameters and heat treatment. Additive Manufacturing, 2019, 30, 100874.	3.0	26
166	On the effect of Re addition on microstructural evolution of a CoNi-based superalloy. Acta Materialia, 2019, 168, 37-51.	7.9	83
167	Unraveling the Metastability of C _{<i>n</i>} ²⁺ (<i>n</i> = 2–4) Clusters. Journal of Physical Chemistry Letters, 2019, 10, 581-588.	4.6	24
168	The effects of carbon on the phase stability and mechanical properties of heat-treated FeNiMnCrAl high entropy alloys. Materials Science & Engineering A: Structural Materials: Properties, Microstructure and Processing, 2019, 748, 59-73.	5.6	23
169	On the compositional partitioning during phase transformation in a binary ferromagnetic MnAl alloy. Acta Materialia, 2019, 174, 227-236.	7.9	25
170	Stability of a model Fe-14Cr nanostructured ferritic alloy after long-term thermal creep. Scripta Materialia, 2019, 170, 134-139.	5.2	11
171	Quantification of solute deuterium in titanium deuteride by atom probe tomography with both laser pulsing and high-voltage pulsing: influence of the surface electric field. New Journal of Physics, 2019, QuastBenni-Level Splitting of <mml:math <="" td="" xmlns:mml="http://www.w3.org/1998/Math/MathML"><td>2.9</td><td>26</td></mml:math>	2.9	26
172	display="inline" overflow="scroll"> <mml:mi>Cu</mml:mi> -Poor and <mml:math xmlns:mml="http://www.w3.org/1998/Math/MathML" display="inline" overflow="scroll"><mml:mi>Cu</mml:mi> -Rich <mml:math xmlns:mml="http://www.w3.org/1998/Math/MathML" display="inline" overflow="scroll"><mml:mi>Cu</mml:mi>CuCuIn<mml:mi></mml:mi></mml:math </mml:math 	3.8	30
173	Microstructural evaluation of a Fe-12Cr nanostructured ferritic alloy designed for impurity sequestration. Journal of Nuclear Materials, 2019, 522, 111-122.	2.7	9
174	Ti and its alloys as examples of cryogenic focused ion beam milling of environmentally-sensitive materials. Nature Communications, 2019, 10, 942.	12.8	89
175	On the origin of a remarkable increase in the strength and stability of an Al rich Al-Ni eutectic alloy by Zr addition. Acta Materialia, 2019, 170, 205-217.	7.9	77
176	Quantification Challenges for Atom Probe Tomography of Hydrogen and Deuterium in Zircaloy-4. Microscopy and Microanalysis, 2019, 25, 481-488.	0.4	33
177	Building a Library of Simulated Atom Probe Data for Different Crystal Structures and Tip Orientations Using TAPSim. Microscopy and Microanalysis, 2019, 25, 320-330.	0.4	7
178	Calibration of Atom Probe Tomography Reconstructions Through Correlation with Electron Micrographs. Microscopy and Microanalysis, 2019, 25, 301-308.	0.4	6
179	An Automated Computational Approach for Complete In-Plane Compositional Interface Analysis by Atom Probe Tomography. Microscopy and Microanalysis, 2019, 25, 389-400.	0.4	16
180	Thermodynamics of grain boundary segregation, interfacial spinodal and their relevance for nucleation during solid-solid phase transitions. Acta Materialia, 2019, 168, 109-120.	7.9	56

#	Article	IF	CITATIONS
181	3D nanostructural characterisation of grain boundaries in atom probe data utilising machine learning methods. PLoS ONE, 2019, 14, e0225041.	2.5	11
182	Imaging individual solute atoms at crystalline imperfections in metals. New Journal of Physics, 2019, 21, 123020.	2.9	26
183	Degradation of iridium oxides <i>via</i> oxygen evolution from the lattice: correlating atomic scale structure with reaction mechanisms. Energy and Environmental Science, 2019, 12, 3548-3555.	30.8	147
184	Influence of composition and precipitation evolution on damage at grain boundaries in a crept polycrystalline Ni-based superalloy. Acta Materialia, 2019, 166, 158-167.	7.9	61
185	Multiscale investigations of nanoprecipitate nucleation, growth, and coarsening in annealed low-Cr oxide dispersion strengthened FeCrAl powder. Acta Materialia, 2019, 166, 1-17.	7.9	46
186	Martensite to austenite reversion in a high-Mn steel: Partitioning-dependent two-stage kinetics revealed by atom probe tomography, in-situ magnetic measurements and simulation. Acta Materialia, 2019, 166, 178-191.	7.9	27
187	Ultrastrong Mediumâ€Entropy Singleâ€Phase Alloys Designed via Severe Lattice Distortion. Advanced Materials, 2019, 31, e1807142.	21.0	301
188	Revealing fracture mechanisms of medium manganese steels with and without delta-ferrite. Acta Materialia, 2019, 164, 683-696.	7.9	108
189	Multi-scale characterization of austenite reversion and martensite recovery in a cold-rolled medium-Mn steel. Acta Materialia, 2019, 166, 512-530.	7.9	67
190	Atomic-scale investigation of hydrogen distribution in a Ti Mo alloy. Scripta Materialia, 2019, 162, 321-325.	5.2	18
191	Elemental site occupancy in the L12 A3B ordered intermetallic phase in Co-based superalloys and its influence on the microstructure. Acta Materialia, 2019, 163, 140-153. Variable chemical decoration of extended defects in Cu-poor <mml:math< td=""><td>7.9</td><td>65</td></mml:math<>	7.9	65
192	xmlns:mml="http://www.w3.org/1998/Math/MathML"> < mml:mrow> < mml:mi mathvariant="normal">C < / mml:mi> < mml:msub> < mml:mi mathvariant="normal">u < / mml:mi> < mml:mn> 2 < / mml:mn> < / mml:msub> < mml:mi> ZnSnS < / mml:mi> < mml:msub> mathvariant="normal">e < / mml:mi> < mml:mn> 4 < / mml:mn> < / mml:msub> < / mml:mrow> < / mml:math> thin	<mml:mi< td=""><td>5</td></mml:mi<>	5
193	films. Physical Review Materials, 2019, 3, . Misorientation-dependent solute enrichment at interfaces and its contribution to defect formation mechanisms during laser additive manufacturing of superalloys. Physical Review Materials, 2019, 3, .	2.4	30
194	Sodium enhances indium-gallium interdiffusion in copper indium gallium diselenide photovoltaic absorbers. Nature Communications, 2018, 9, 826.	12.8	51
195	Competition between formation of carbides and reversed austenite during tempering of a medium-manganese steel studied by thermodynamic-kinetic simulations and atom probe tomography. Acta Materialia, 2018, 147, 165-175.	7.9	60
196	Warm ductility enhanced by austenite reversion in ultrafine-grained duplex steel. Acta Materialia, 2018, 148, 344-354.	7.9	22
197	Impact of local electrostatic field rearrangement on field ionization. Journal Physics D: Applied Physics, 2018, 51, 105601.	2.8	20
198	On the grain boundary strengthening effect of boron in γ/γ′ Cobalt-base superalloys. Acta Materialia, 2018, 145, 247-254.	7.9	73

#	Article	IF	CITATIONS
199	Microstructural degradation of polycrystalline superalloys from oxidized carbides and implications on crack initiation. Scripta Materialia, 2018, 147, 59-63.	5.2	49
200	Ag-Segregation to Dislocations in PbTe-Based Thermoelectric Materials. ACS Applied Materials & Interfaces, 2018, 10, 3609-3615.	8.0	74
201	Atomic-scale insights into surface species of electrocatalysts in three dimensions. Nature Catalysis, 2018, 1, 300-305.	34.4	161
202	Synthesis and stabilization of a new phase regime in a Mo-Si-B based alloy by laser-based additive manufacturing. Acta Materialia, 2018, 151, 31-40.	7.9	42
203	On the detection of multiple events in atom probe tomography. Ultramicroscopy, 2018, 189, 54-60.	1.9	59
204	Correlative Microscopy—Novel Methods and Their Applications to Explore 3D Chemistry and Structure of Nanoscale Lattice Defects: A Case Study in Superalloys. Jom, 2018, 70, 1736-1743.	1.9	49
205	Phase nucleation through confined spinodal fluctuations at crystal defects evidenced in Fe-Mn alloys. Nature Communications, 2018, 9, 1137.	12.8	101
206	Characterizing solute hydrogen and hydrides in pure and alloyed titanium at the atomic scale. Acta Materialia, 2018, 150, 273-280.	7.9	81
207	Advanced data mining in field ion microscopy. Materials Characterization, 2018, 146, 307-318.	4.4	10
208	The effect of chromium and cobalt segregation at dislocations on nickel-based superalloys. Scripta Materialia, 2018, 145, 76-80.	5.2	132
209	Hot cracking mechanism affecting a non-weldable Ni-based superalloy produced by selective electron Beam Melting. Acta Materialia, 2018, 142, 82-94.	7.9	344
210	Correlative transmission <scp>Kikuchi</scp> diffraction and atom probe tomography study of <scp>Cu(In,Ga)Se₂</scp> grain boundaries. Progress in Photovoltaics: Research and Applications, 2018, 26, 196-204.	8.1	36
211	Enhanced strength and ductility in a high-entropy alloy via ordered oxygen complexes. Nature, 2018, 563, 546-550.	27.8	988
212	Interfaces and defect composition at the near-atomic scale through atom probe tomography investigations. Journal of Materials Research, 2018, 33, 4018-4030.	2.6	35
213	The Laplace Project: An integrated suite for preparing and transferring atom probe samples under cryogenic and UHV conditions. PLoS ONE, 2018, 13, e0209211.	2.5	57
214	A near atomic-scale view at the composition of amyloid-beta fibrils by atom probe tomography. Scientific Reports, 2018, 8, 17615.	3.3	20
215	On the segregation of Re at dislocations in the γ' phase of Ni-based single crystal superalloys. Materialia, 2018, 4, 109-114.	2.7	51
216	Conventional vs harmonic-structured β-Ti-25Nb-25Zr alloys: A comparative study of deformation mechanisms. Acta Materialia, 2018, 161, 420-430.	7.9	37

#	Article	IF	CITATIONS
217	Tailoring Thermoelectric Transport Properties of Ag-Alloyed PbTe: Effects of Microstructure Evolution. ACS Applied Materials & Interfaces, 2018, 10, 38994-39001.	8.0	17
218	Why Tinâ€Doping Enhances the Efficiency of Hematite Photoanodes for Water Splitting—The Full Picture. Advanced Functional Materials, 2018, 28, 1804472.	14.9	53
219	Cluster hardening in Al-3Mg triggered by small Cu additions. Acta Materialia, 2018, 161, 12-20.	7.9	28
220	Thermophysical and Mechanical Properties of Advanced Single Crystalline Co-base Superalloys. Metallurgical and Materials Transactions A: Physical Metallurgy and Materials Science, 2018, 49, 4099-4109.	2.2	58
221	Elemental partitioning and site-occupancy in γ/γ′ forming Co-Ti-Mo and Co-Ti-Cr alloys. Scripta Materialia, 2018, 154, 159-162.	5.2	44
222	Elemental segregation to twin boundaries in a MnAl ferromagnetic Heusler alloy. Scripta Materialia, 2018, 155, 144-148.	5.2	18
223	Sulfur – induced embrittlement in high-purity, polycrystalline copper. Acta Materialia, 2018, 156, 64-75.	7.9	13
224	Segregation assisted grain boundary precipitation in a model Al-Zn-Mg-Cu alloy. Acta Materialia, 2018, 156, 318-329.	7.9	189
225	Nano-laminated thin film metallic glass design for outstanding mechanical properties. Scripta Materialia, 2018, 155, 73-77.	5.2	23
226	Atom probe tomography analysis of the reference zircon gj-1: An interlaboratory study. Chemical Geology, 2018, 495, 27-35.	3.3	27
227	Launching Materialia. Acta Biomaterialia, 2018, 75, 1-2.	8.3	3
228	Strain-Induced Asymmetric Line Segregation at Faceted Si Grain Boundaries. Physical Review Letters, 2018, 121, 015702.	7.8	65
229	Effects of Carbon Variation on Microstructure Evolution in Weld Heat-Affected Zone of Nb-Ti Microalloyed Steels. Metallurgical and Materials Transactions A: Physical Metallurgy and Materials Science, 2018, 49, 4824-4837.	2.2	9
230	Machine-learning-based atom probe crystallographic analysis. Ultramicroscopy, 2018, 194, 15-24.	1.9	14
231	Atomic scale analysis of grain boundary deuteride growth front in Zircaloy-4. Scripta Materialia, 2018, 156, 42-46.	5.2	40
232	Reversion to Ultrafine-Grained Austenite in a Medium-Mn AHSS. Microscopy and Microanalysis, 2018, 24, 2228-2229.	0.4	0
233	Elemental segregation to antiphase boundaries in a crept CoNi-based single crystal superalloy. Scripta Materialia, 2018, 157, 62-66.	5.2	48
234	Parameter free quantitative analysis of atom probe data by correlation functions: Application to the precipitation in Al-Zn-Mg-Cu. Scripta Materialia, 2018, 154, 106-110.	5.2	55

#	Article	IF	CITATIONS
235	The Role of Oxidized Carbides on Thermal-Mechanical Performance of Polycrystalline Superalloys. Metallurgical and Materials Transactions A: Physical Metallurgy and Materials Science, 2018, 49, 4236-4245.	2.2	30
236	On the diffusive phase transformation mechanism assisted by extended dislocations during creep of a single crystal CoNi-based superalloy. Acta Materialia, 2018, 155, 362-371.	7.9	89
237	Tetragonal fcc-Fe induced by κ -carbide precipitates: Atomic scale insights from correlative electron microscopy, atom probe tomography, and density functional theory. Physical Review Materials, 2018, 2, .	2.4	14
238	Interstitial atoms enable joint twinning and transformation induced plasticity in strong and ductile high-entropy alloys. Scientific Reports, 2017, 7, 40704.	3.3	279
239	Evaluation of Analysis Conditions for Laser-Pulsed Atom Probe Tomography: Example of Cemented Tungsten Carbide. Microscopy and Microanalysis, 2017, 23, 431-442.	0.4	19
240	Investigation of solute/interphase interaction during ferrite growth. Acta Materialia, 2017, 124, 536-543.	7.9	32
241	Correlating Atom Probe Tomography with Atomic-Resolved Scanning Transmission Electron Microscopy: Example of Segregation at Silicon Grain Boundaries. Microscopy and Microanalysis, 2017, 23, 291-299.	0.4	24
242	Nanoscale Stoichiometric Analysis of a High-Temperature Superconductor by Atom Probe Tomography. Microscopy and Microanalysis, 2017, 23, 414-424.	0.4	18
243	A nexus between 3D atomistic data hybrids derived from atom probe microscopy and computational materials science: A new analysis of solute clustering in Al-alloys. Scripta Materialia, 2017, 131, 93-97.	5.2	19
244	Reflections on the Projection of Ions in Atom Probe Tomography. Microscopy and Microanalysis, 2017, 23, 238-246.	0.4	29
245	Ultrastrong steel via minimal lattice misfit and high-density nanoprecipitation. Nature, 2017, 544, 460-464.	27.8	843
246	Effect of Nb Addition to Ti-Bearing Super Martensitic Stainless Steel on Control of Austenite Grain Size and Strengthening. Metallurgical and Materials Transactions A: Physical Metallurgy and Materials Science, 2017, 48, 2460-2471.	2.2	16
247	Atomic diffusion induced degradation in bimetallic layer coated cemented tungsten carbide. Corrosion Science, 2017, 120, 1-13.	6.6	18
248	Automated Atom-By-Atom Three-Dimensional (3D) Reconstruction of Field Ion Microscopy Data. Microscopy and Microanalysis, 2017, 23, 255-268.	0.4	16
249	Core-shell nanoparticle arrays double the strength of steel. Scientific Reports, 2017, 7, 42547.	3.3	60
250	Cd and Impurity Redistribution at the CdS/CIGS Interface After Annealing of CIGS-Based Solar Cells Resolved by Atom Probe Tomography. IEEE Journal of Photovoltaics, 2017, 7, 313-321.	2.5	19
251	On the Multiple Event Detection in Atom Probe Tomography. Microscopy and Microanalysis, 2017, 23, 618-619.	0.4	12
252	Degradation Mechanism of Molds for Precision Glass Molding. Microscopy and Microanalysis, 2017, 23, 698-699.	0.4	1

#	Article	IF	CITATIONS
253	A New Approach to Understand the Adsorption of Thiophene on Different Surfaces: An Atom Probe Investigation of Self-Assembled Monolayers. Langmuir, 2017, 33, 9573-9581.	3.5	11
254	A Methodology for Investigation of Grain-Boundary Diffusion and Segregation. Microscopy and Microanalysis, 2017, 23, 656-657.	0.4	1
255	Paths to Open Access: An update from Acta Materialia, Inc Acta Biomaterialia, 2017, 60, 1-2.	8.3	0
256	In-process Precipitation During Laser Additive Manufacturing Investigated by Atom Probe Tomography. Microscopy and Microanalysis, 2017, 23, 694-695.	0.4	22
257	Strengthening and strain hardening mechanisms in a precipitation-hardened high-Mn lightweight steel. Acta Materialia, 2017, 140, 258-273.	7.9	179
258	High Fidelity Reconstruction of Experimental Field Ion Microscopy Data by Atomic Relaxation Simulations. Microscopy and Microanalysis, 2017, 23, 642-643.	0.4	5
259	Applications, Technical Challenges, and Recent Implementation of a UHV/Cryogenic Specimen Transfer System for Atom Probe Tomography. Microscopy and Microanalysis, 2017, 23, 622-623.	0.4	3
260	Atomistic Simulations of Surface Effects Under High Electric Fields. Microscopy and Microanalysis, 2017, 23, 644-645.	0.4	1
261	Improved Atom Probe Methodology for Studying Carbon Redistribution in Low-Carbon High-Ms Lath Martensitic Steels. Microscopy and Microanalysis, 2017, 23, 706-707.	0.4	4
262	Correlative Transmission EBSD-APT Analysis of Grain Boundaries in Cu(In,Ga)Se ₂ and Cu ₂ ZnSnSe ₄ Based Thin-film Solar Cells. Microscopy and Microanalysis, 2017, 23, 672-673.	0.4	1
263	Elemental distribution in the martensite–austenite constituent in intercritically reheated coarse-grained heat-affected zone of a high-strength pipeline steel. Scripta Materialia, 2017, 139, 67-70.	5.2	64
264	Confined chemical and structural states at dislocations in Fe-9wt%Mn steels: A correlative TEM-atom probe study combined with multiscale modelling. Acta Materialia, 2017, 124, 305-315.	7.9	73
265	Insights into microstructural interfaces in aerospace alloys characterised by atom probe tomography. Materials Science and Technology, 2016, 32, 232-241.	1.6	20
266	Behavior of molecules and molecular ions near a field emitter. New Journal of Physics, 2016, 18, 033031.	2.9	130
267	Recognizing 60 years of achievements in field emission and atomic scale microscopy. Materials Today, 2016, 19, 182-183.	14.2	1
268	The influence of crystal structure on ion-irradiation tolerance in the Sm(x)Yb(2-x)TiO5 series. Journal of Nuclear Materials, 2016, 471, 17-24.	2.7	15
269	A Brief Overview of Atom Probe Tomography Research. Applied Microscopy, 2016, 46, 117-126.	1.4	24
270	Mining information from atom probe data. Ultramicroscopy, 2015, 159, 324-337.	1.9	50

#	Article	IF	CITATIONS
271	A new systematic framework for crystallographic analysis of atom probe data. Ultramicroscopy, 2015, 154, 7-14.	1.9	27
272	Crystal chemistry of the orthorhombic Ln2TiO5 compounds with Ln=La, Pr, Nd, Sm, Gd, Tb and Dy. Journal of Solid State Chemistry, 2015, 227, 60-67.	2.9	18
273	Imaging of radiation damage using complementary field ion microscopy and atom probe tomography. Ultramicroscopy, 2015, 159, 387-394.	1.9	18
274	Ion-irradiation resistance of the orthorhombic Ln2TiO5 (LnÂ=ÂLa, Pr, Nd, Sm, Eu, Gd, Tb and Dy) series. Journal of Nuclear Materials, 2015, 467, 683-691.	2.7	20
275	From solid solution to cluster formation of Fe and Cr in $\hat{I}\pm$ -Zr. Journal of Nuclear Materials, 2015, 467, 320-331.	2.7	23
276	Interpreting atom probe data from chromium oxide scales. Ultramicroscopy, 2015, 159, 354-359.	1.9	29
277	The effect orientation of features in reconstructed atom probe data on the resolution and measured composition of T1 plates in an A2198 aluminium alloy. Ultramicroscopy, 2015, 159, 368-373.	1.9	2
278	Restoring the lattice of Si-based atom probe reconstructions for enhanced information on dopant positioning. Ultramicroscopy, 2015, 159, 314-323.	1.9	19
279	Crystal structures of orthorhombic, hexagonal, and cubic compounds of the Sm(x)Yb(2â^'x)TiO5 series. Journal of Solid State Chemistry, 2014, 213, 182-192.	2.9	31
280	Microstructural evolution during ageing of Al–Cu–Li–x alloys. Acta Materialia, 2014, 66, 199-208.	7.9	183
281	Atomically resolved tomography to directly inform simulations for structure–property relationships. Nature Communications, 2014, 5, 5501.	12.8	53
282	On the roles of graphene oxide doping for enhanced supercurrent in MgB ₂ based superconductors. Nanoscale, 2014, 6, 6166-6172.	5.6	40
283	Resolving the Morphology of Niobium Carbonitride Nano-Precipitates in Steel Using Atom Probe Tomography. Microscopy and Microanalysis, 2014, 20, 1100-1110.	0.4	30
284	Electrostatic simulations of a local electrode atom probe: The dependence of tomographic reconstruction parameters on specimen and microscope geometry. Ultramicroscopy, 2013, 132, 107-113.	1.9	53
285	Reconstructing atom probe data: A review. Ultramicroscopy, 2013, 132, 19-30.	1.9	126
286	Atom probe tomography spatial reconstruction: Status and directions. Current Opinion in Solid State and Materials Science, 2013, 17, 236-247.	11.5	122
287	The rise of computational techniques in atom probe microscopy. Current Opinion in Solid State and Materials Science, 2013, 17, 224-235.	11.5	25
288	Quantitative dopant distributions in GaAs nanowires using atom probe tomography. Ultramicroscopy, 2013, 132, 186-192.	1.9	29

#	Article	IF	CITATIONS
289	Full tip imaging in atom probe tomography. Ultramicroscopy, 2013, 124, 96-101.	1.9	23
290	Spatial decomposition of molecular ions within 3D atom probe reconstructions. Ultramicroscopy, 2013, 132, 92-99.	1.9	5
291	Influence of experimental parameters on the composition of precipitates in metallic alloys. Ultramicroscopy, 2013, 132, 199-204.	1.9	5
292	Atom probe microscopy characterization of as quenched Zr–0.8wt% Fe and Zr–0.15wt% Cr binary alloys. Materials Letters, 2013, 91, 63-66.	2.6	9
293	Correlating spatial, temporal and chemical information in atom probe data: new insights from multiple evaporation in microalloyed steels. Philosophical Magazine Letters, 2013, 93, 299-306.	1.2	9
294	Nearest neighbour diagnostic statistics on the accuracy of APT solute cluster characterisation. Philosophical Magazine, 2013, 93, 975-989.	1.6	15
295	A Weibull Perspective on the Fracture of Atom Probe Specimens. Microscopy and Microanalysis, 2013, 19, 996-997.	0.4	33
296	Atom Probe Characterization of Corroded Alloy 600. Microscopy and Microanalysis, 2013, 19, 1020-1021.	0.4	1
297	Simulation-Enhanced Atom Probe for Complete 3D Atomistic Imaging. Microscopy and Microanalysis, 2013, 19, 998-999.	0.4	0
298	Compositional nonuniformities in pulsed laser atom probe tomography analysis of compound semiconductors. Journal of Applied Physics, 2012, 111, 064908.	2.5	35
299	Interfacial chemistry in an InAs/GaSb superlattice studied by pulsed laser atom probe tomography. Applied Physics Letters, 2012, 100, .	3.3	23
300	Quantification of the zinc dopant concentration in GaAs nanowires. , 2012, , .		0
301	Atom probe crystallography. Materials Today, 2012, 15, 378-386.	14.2	158
302	Atom Probe Microscopy. Springer Series in Materials Science, 2012, , .	0.6	501
303	A New Approach to the Determination of Concentration Profiles in Atom Probe Tomography. Microscopy and Microanalysis, 2012, 18, 359-364.	0.4	40
304	Phase separation in thick InGaN layers – A quantitative, nanoscale study by pulsed laser atom probe tomography. Acta Materialia, 2012, 60, 4277-4285.	7.9	31
305	Atom probe microscopy investigation of Mg site occupancy within Î′′ precipitates in an Al–Mg–Li alloy. Scripta Materialia, 2012, 66, 903-906.	5.2	65
306	Atom probe crystallography: Atomic-scale 3-D orientation mapping. Scripta Materialia, 2012, 66, 907-910.	5.2	57

#	Article	IF	CITATIONS
307	Impact of directional walk on atom probe microanalysis. Ultramicroscopy, 2012, 113, 182-191.	1.9	135
308	Overcoming challenges in the study of nitrided microalloyed steels using atom probe. Ultramicroscopy, 2012, 112, 32-38.	1.9	15
309	Field Ion Microscopy. Springer Series in Materials Science, 2012, , 9-28.	0.6	1
310	From Field Desorption Microscopy to Atom Probe Tomography. Springer Series in Materials Science, 2012, , 29-68.	0.6	3
311	Specimen Preparation. Springer Series in Materials Science, 2012, , 71-110.	0.6	6
312	Experimental Protocols in Atom Probe Tomography. Springer Series in Materials Science, 2012, , 121-155.	0.6	2
313	Tomographic Reconstruction. Springer Series in Materials Science, 2012, , 157-209.	0.6	4
314	Analysis Techniques for Atom Probe Tomography. Springer Series in Materials Science, 2012, , 213-297.	0.6	7
315	Atom Probe Microscopy and Materials Science. Springer Series in Materials Science, 2012, , 299-311.	0.6	2
316	Estimating the physical clusterâ€size distribution within materials using atomâ€probe. Microscopy Research and Technique, 2011, 74, 799-803.	2.2	24
317	A Lattice-Rectified and Detection Efficiency Compensated APT Reconstruction. Microscopy and Microanalysis, 2011, 17, 722-723.	0.4	2
318	Accuracy of pulsed laser atom probe tomography for compound semiconductor analysis. Journal of Physics: Conference Series, 2011, 326, 012031.	0.4	24
319	Dynamic reconstruction for atom probe tomography. Ultramicroscopy, 2011, 111, 1619-1624.	1.9	72
320	Nickel segregation on dislocation loops in implanted silicon. Scripta Materialia, 2011, 64, 378-381.	5.2	40
321	Advances in the reconstruction of atom probe tomography data. Ultramicroscopy, 2011, 111, 448-457.	1.9	209
322	Optimisation of mass ranging for atom probe microanalysis and application to the corrosion processes in Zr alloys. Ultramicroscopy, 2011, 111, 480-486.	1.9	44
323	Atom probe crystallography: Characterization of grain boundary orientation relationships in nanocrystalline aluminium. Ultramicroscopy, 2011, 111, 493-499.	1.9	51
324	Some aspects of the field evaporation behaviour of GaSb. Ultramicroscopy, 2011, 111, 487-492.	1.9	77

#	Article	lF	CITATIONS
325	Atom probe tomography and transmission electron microscopy characterisation of precipitation in an Al–Cu–Li–Mg–Ag alloy. Ultramicroscopy, 2011, 111, 683-689.	1.9	96
326	Atom probe tomography of reactor pressure vessel steels: An analysis of data integrity. Ultramicroscopy, 2011, 111, 676-682. Direct Observation of Local Potassium Variation and its Correlation to Electronic Inhomogeneity.	1.9	38
327	in <mml:math display="inline" xmlns:mml="http://www.w3.org/1998/Math/MathML"><mml:mo´ stretchy="false">(<mml:msub><mml:mi>Ba</mml:mi><mml:mrow><mml:mn>1</mml:mn><mm< td=""><td>l:mo>â^'7.8</td><td>nl:mo><mml: 48</mml: </td></mm<></mml:mrow></mml:msub></mml:mo´ </mml:math>	l:mo>â^'7.8	nl:mo> <mml: 48</mml:
328	Physical Review Letters, 2011, 106, 247002. Bringing Standardized Processes to Atom-Probe Tomography - Part 1: Establishing Standardized Terminology. Microscopy and Microanalysis, 2011, 17, 858-859.	0.4	0
329	Influence of the wavelength on the spatial resolution of pulsed-laser atom probe. Journal of Applied Physics, 2011, 110, .	2.5	16
330	Lattice Rectification in Atom Probe Tomography: Toward True Three-Dimensional Atomic Microscopy. Microscopy and Microanalysis, 2011, 17, 226-239.	0.4	58
331	Optimization of pulsed laser atom probe (PLAP) for the analysis of nanocomposite Ti–Si–N films. Ultramicroscopy, 2010, 110, 836-843.	1.9	60
332	Impact of laser pulsing on the reconstruction in an atom probe tomography. Ultramicroscopy, 2010, 110, 1215-1222.	1.9	51
333	Microstructural investigation of Ti–Si–N hard coatings. Scripta Materialia, 2010, 63, 192-195.	5.2	27
334	High-resolution nanostructural investigation of Zn4Sb3 alloys. Scripta Materialia, 2010, 63, 784-787.	5.2	36
335	Challenges Associated with the Characterisation of Nanocrystalline Materials Using Atom Probe Tomography. Materials Science Forum, 2010, 654-656, 2366-2369.	0.3	5
336	Influence of surface migration on the spatial resolution of pulsed laser atom probe tomography. Journal of Applied Physics, 2010, 108, .	2.5	81
337	Spatial Resolution in Atom Probe Tomography. Microscopy and Microanalysis, 2010, 16, 99-110.	0.4	153
338	On the multiplicity of field evaporation events in atom probe: A new dimension to the analysis of mass spectra. Philosophical Magazine Letters, 2010, 90, 121-129.	1.2	96
339	Atom Probe Microscopy of Self-Assembled Monolayers: Preliminary Results. Langmuir, 2010, 26, 5291-5294.	3.5	28
340	Advances in the calibration of atom probe tomographic reconstruction. Journal of Applied Physics, 2009, 105, .	2.5	214
341	Qualification of the tomographic reconstruction in atom probe by advanced spatial distribution map techniques. Ultramicroscopy, 2009, 109, 815-824.	1.9	129
342	On the understanding of the microscopic origin of the properties of diluted magnetic semiconductors by atom probe tomography. Journal of Magnetism and Magnetic Materials, 2009, 321, 935-943.	2.3	12

#	Article	lF	CITATIONS
343	Light Output Improvement of Oxide-Textured InGaN-Based Light-Emitting Diodes by Bias-Assisted Photoelectrochemical Oxidation With Imprint Technique. IEEE Photonics Technology Letters, 2009, 21, 718-720.	2.5	5
344	Origin of the spatial resolution in atom probe microscopy. Applied Physics Letters, 2009, 95, 034103.	3.3	80
345	Applications of Spatial Distribution Maps for Advanced Atom Probe Reconstruction and Data Analysis. Microscopy and Microanalysis, 2009, 15, 246-247.	0.4	12
346	Tomographic Reconstruction in Atom Probe Microscopy: Past, Present.Â.Â. Future?. Microscopy and Microanalysis, 2009, 15, 10-11.	0.4	8
347	Investigation of Self-assembled Monolayer by Atom Probe Microscopy. Microscopy and Microanalysis, 2009, 15, 272-273.	0.4	34
348	Promoting Standards in Quantitative Atom Probe Tomography Analysis. Microscopy and Microanalysis, 2009, 15, 260-261.	0.4	5
349	Estimation of the Reconstruction Parameters for Atom Probe Tomography. Microscopy and Microanalysis, 2008, 14, 296-305.	0.4	143
350	Alternating current bias-assisted photoenhanced oxidation of n-GaN in dionized water. Optoelectronic and Microelectronic Materials and Devices (COMMAD), Conference on, 2008, , .	0.0	1
351	Determination of the tip temperature in laser assisted atom-probe tomography using charge state distributions. Journal of Applied Physics, 2008, 104, .	2.5	52
352	Atom Probe Tomography at The University of Sydney. Advances in Materials Research, 2008, , 187-216.	0.2	2
353	Ultrafast Laser Assisted Field Evaporation and Atom Probe Tomography Applications. Journal of Physics: Conference Series, 2007, 59, 132-135.	0.4	5
354	Correlated field evaporation as seen by atom probe tomography. Surface Science, 2007, 601, 536-543.	1.9	110
355	Optical and thermal processes involved in ultrafast laser pulse interaction with a field emitter. Ultramicroscopy, 2007, 107, 713-719.	1.9	23
356	Toward a laser assisted wide-angle tomographic atom-probe. Surface and Interface Analysis, 2007, 39, 278-282.	1.8	71
357	Design of a femtosecond laser assisted tomographic atom probe. Review of Scientific Instruments, 2006, 77, 043705.	1.3	295
358	Evidence of Field Evaporation Assisted by Nonlinear Optical Rectification Induced by Ultra Fast Laser. , 2006, , .		0
359	First steps in ultrafast laser assisted atom probe tomography. , 2006, , .		0
360	Evidence of field evaporation assisted by nonlinear optical rectification induced by ultrafast laser. Physical Review B, 2006, 73, .	3.2	57

#	Article	IF	CITATIONS
361	Estimation of the cooling times for a metallic tip under laser illumination. Applied Physics Letters, 2006, 88, 094105.	3.3	72
362	Investigation of an oxide layer by femtosecond-laser-assisted atom probe tomography. Applied Physics Letters, 2006, 88, 114101.	3.3	49
363	Design of a Wide Angle Laser Assited Tomographic Atom Probe. , 2006, , .		1
364	Laser Atom Probe Tomography: some applications. , 2006, , .		0
365	Estimation of the tip field enhancement on a field emitter under laser illumination. Applied Physics Letters, 2005, 86, 094101.	3.3	84
366	Tip-field-enhancement characterisation by field ion microscopy. , 0, , .		0
367	Complementarity of Atom Probe, Small Angle Scattering and Differential Scanning Calorimetry for the Study of Precipitation in Aluminium Alloys. Materials Science Forum, 0, 794-796, 926-932.	0.3	10
368	Hydrogen and deuterium charging of site-specific specimen for atom probe tomography. Open Research Europe, 0, 1, 122.	2.0	3
369	Hydrogen and deuterium charging of lifted-out specimens for atom probe tomography. Open Research Europe, 0, 1, 122.	2.0	6